Vol. 2, *Astrodynamics and Astrionics*, Pergamon Press, PWN—Polish Scientific Publishers, 1970.

[4] Fletcher, R. and Powell, M. J. D., "A Rapidly Convergent Descent Method for Minimization," *The Computer Journal*, Vol. 6, No. 2, July 1963, pp. 163–168.

[5] Johnson, I. L., "Impulsive Orbit Transfer Optimization by an Accelerated Gradient Method," *Journal of Spacecraft and Rockets*, Vol. 6, No. 5, May 1969, pp. 630–632.

An Empirical Model of the Motion of Turbulent Vortex Rings

GARY M. JOHNSON*
Aerospace Research Laboratories, Wright-Patterson Air Force Base, Ohio

DIMENSIONAL arguments indicate that the motion of both axial turbulent puffs (strongly turbulent masses of fluid moving through surroundings with which they readily mix)[1] and turbulent vortex rings[2] will remain similar at all distances from their virtual sources if their spreading rates are linear and their translational velocities decay as the inverse cube of the distance from their respective virtual sources.

This hypothesis appears to be well substantiated for the case of the rapidly spreading turbulent puffs.[1,3] However, the validity of the model is much more difficult to determine for the case of the vortex ring, where the extremely slow ring growth leads to the prediction of very large virtual origins. In fact, recent experiments[4] indicate that measurements would be required at least 1000 diam from the discharging orifice, in order to satisfactorily test the similarity model. Since such measurements have not been made and do not appear to be in the offing, the following empirical model is proposed for use in engineering calculations. Quantitative agreement with experimental results is good to distances on the order of 70 diam from the discharging orifice.

The model is based on measurements of air vortex rings, seeded with a mist of dioctyl phthalate droplets, traveling through quiescent air. The time of flight was recorded by using the signal from a hot-wire anemometer to stop an electronic event timer as the vortex passed the anemometer. The hot-wire circuitry was also used to flash a stroboscope, thereby illuminating the vortex to an open-lensed camera, which recorded its geometry. All measurements were repeated at least thirty times and the mean values were used in further computations.

It was apparent from the data that the behavior of the rings is very accurately described by

$$(t - t_v)/t_0 = C[(x - x_v)/D]^{3/2} \qquad (1)$$

Table 1 Numerical values for the various parameters in Eqs. (1) and (2)

Case	Symbol	D(in.)	Volume of Efflux ($in.^3$)	t_0(sec)	t_v(sec)	x_v(in.)	C	K
1	⊙	4	157.00	.033	.028	-3.781	.131	.943
2	△	4	157.00	.036	-.007	-14.660	.165	.959
3	×	4	78.50	.019	.017	-3.941	.230	.828
4	⊡	4	78.50	.021	.001	15.870	.337	.890
5	▱	4	39.25	.015	.083	7.505	.507	.726

Received December 9, 1970.

* Research Aerodynamicist, Energetics Research Laboratory.

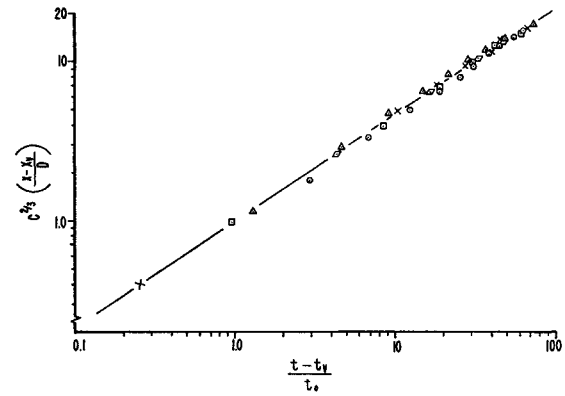

Fig. 1 Comparison of time of flight data with Eq. (1) see Table 1 for an explanation of the symbology.

and

$$2R/D = K[(x - x_v)/D]^{1/6} \qquad (2)$$

where t_v and x_v represent some virtual time and distance respectively, t_0 is the characteristic vortex generation time, R is the vortex ring radius, D is the diameter of the generating orifice, and C and K are constants.

The values of the various parameters for the different initial conditions tested are presented in Table 1. Possible differences between the geometric and kinematic virtual origins of the type discussed by Flora and Goldschmidt[5] have been ignored for the present study. Geometric virtual origins are used throughout.

Quite pleasantly, it may be observed that the values of the virtual time and distance are small. The same data, when fitted to the similarity model, yielded virtual origins for both time and distance which were on the order of the maximum time and distance recorded in the experiments. The small virtual origins obtained when the empirical model is used mean that this model is much less sensitive to small errors in the determination of these virtual origins than is the similarity model.

The data are compared to Eqs. (1) and (2) in Figs. 1 and 2, respectively. As may be observed, the agreement is quite good. The present results have been qualitatively compared to other existing data.[6–8] The agreement is good, except with the data of Krutzsch.[7] However, his results must be viewed skeptically as the measurements were made in an extremely confined chamber.

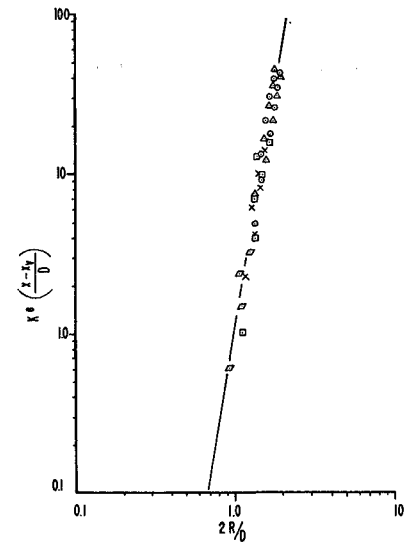

Fig. 2 Comparison of vortex ring radius data with Eq. (2); see Table I for an explanation of the symbology.

In summary, Eqs. (1) and (2) provide a quite good empirical model for the behavior of turbulent vortex rings and are valid to reasonably large distances from the discharging orifice. The equations also have the virtue of involving very small virtual times and distances and hence are not overly sensitive to inaccuracies in the determination of these quantities.

References

[1] Richards, J. M., "Puff Motions in Unstratified Surroundings," *Journal of Fluid Mechanics*, Vol. 21, Pt. 1, 1965, pp. 97–106.

[2] Turner, J. S., "Buoyant Vortex Rings," *Proceedings of the Royal Society of London, Series A*, Vol. 239, 1957, pp. 61–75.

[3] Grigg, H. R. and Stewart, R. W., "Turbulent Diffusion in a Stratified Fluid," *Journal of Fluid Mechanics*, Vol. 15, Pt. 1, 1963, pp. 174–186.

[4] Johnson, G. M., "Researches on the Propagation and Decay of Vortex Rings," Rept. ARL 70-0093,1970 Aerospace Research Labs., Wright-Patterson Air Force Base, Ohio.

[5] Flora, J. J., Jr. and Goldschmidt, V. W., "Virtual Origins of a Free Plane Turbulent Jet," *AIAA Journal*, Vol. 7, No. 12, Dec. 1969, pp. 2344–2346.

[6] Banerji, K. and Barave, R. V., "On Oberbeck's Vorticies," *Philosophical Magazine*, Vol. 11, 1931, pp. 1057–1081.

[7] Krutzsch, C. H., "Uber Eine Experimentell Beobachtete Erscheinung an Wirbelringen Bei Ihrer Translatorischen Bewegung in Wirklichen Flussingkeiten," *Analen der Physik*, Ser. 5, Vol. 35, 1939, pp. 497–523.

[8] Sadron, M., "Contribution A L'etude de la Formation et de la Propagation des Anneaux de Tourbillion Dans L'air," *Journal de Physique*, Vol. 7, No. 3, 1926, pp. 76–91.

Eddy Viscosity Distributions in a Mach 20 Turbulent Boundary Layer

D. M. Bushnell* and D. J. Morris†

NASA Langley Research Center, Hampton, Va.

Nomenclature

A = damping scale, Eq. (4)
A^* = damping constant, Eq. (5)
C_f = skin friction coefficient
K = "Prandtl wall slope" on mixing length, Eq. (4)
l = Prandtl mixing length
M = Mach number
P = pressure
R_θ = Reynolds number based on compressible momentum thickness
r = radius
T_w = wall temperature
T_t = freestream stagnation temperature
u,v = longitudinal and normal velocity components, respectively
x,y = cartesian coordinates along and normal to the nozzle wall, respectively
δ^* = compressible displacement thickness
δ_i^* = incompressible displacement thickness
ρ = density
δ^+ = $\rho_w\delta(\tau_w/\rho_w)^{1/2}/\mu_w$
τ = shear stress
ϵ = eddy viscosity
μ = molecular viscosity
δ = density boundary-layer thickness, y at $\rho/\rho_e = 0.995$

Subscripts

e = local value external to boundary layer
w = wall value

Received December 3, 1970; revision received January 11, 1971.

* Head, Viscous Flows Section, Hypersonic Vehicles Division. Member AIAA.

† Aerospace Technologist, Viscous Flows Section, Hypersonic Vehicles Division.

MOST current methods for computing compressible turbulent boundary-layers rely upon some assumed model of the turbulent shear or Reynolds stress term which appears in the momentum equation for the mean flow. Assumed models can be validated in two ways; one can either compute results for various test cases and compare these with experimental profiles, or one can work backward from the experimental data using the mean flow equations and directly compare the resulting shear stress and eddy viscosity distributions with the assumed model. The latter method has been utilized in several investigations[1–4] up to a Mach number of 7. The results of this work, particularly Refs. 2 and 4, greatly aided the development of computational techniques for compressible turbulent boundary layers. Recently, detailed nozzle boundary-layer profile data at several longitudinal stations became available in the Mach 20 range.[5] This Note presents shear stress and eddy viscosity distributions obtained from this high Mach number profile data and indicates the most consistent of the available models for turbulent shear.

The comparisons shown in Ref. 5 prompted this work by indicating that the method of Ref. 6 was unable to predict observed velocity profile development at Mach 20 (Fig. 6 of Ref. 5). This data provide a severe test of "compressibility effects" upon turbulent shear models because of the large density change (factor of 140) across the boundary layer. As the data of Ref. 5 were obtained on the inside wall of an axisymmetric nozzle, the following mean flow equations are used

Continuity

$$\partial(\rho ur)/\partial x + \partial(\rho vr)/\partial y = 0 \tag{1}$$

Momentum

$$\partial(\rho u^2 r)/\partial x + \partial(\rho uvr)/\partial y = -r(dPe/dx) + \partial(r\tau)/\partial y \tag{2}$$

where $r = r_w - y$ and $\tau = (\mu + \epsilon)(du/dy)$.

In the usual fashion an expression for ρvr obtained by integrating Eq. (1) is substituted into Eq. (2) and Eq. (2) integrated once with respect to y. Then, u/u_e and ρ/ρ_e are assumed to be functions of y/δ only[4] (a fairly accurate assumption for the data of Ref. 5).

The resulting equation follows:

$$\frac{\tau}{\rho_e u_e^2}\left(1 - \frac{y}{r_w}\right) = \frac{C_f}{2} + \int_0^{y/\delta} \frac{\rho}{\rho_e}\left(\frac{u}{u_e}\right)^2 dy/\delta \times \left[\frac{\delta}{\rho_e u_e^2}\frac{d(\rho_e u_e^2)}{dx} + \frac{d\delta}{dx} + \frac{\delta}{r_w}\frac{dr_w}{dx}\right] - \int_0^{y/\delta} y/\delta \times \frac{\rho}{\rho_e}\left(\frac{u}{u_e}\right)^2 dy/\delta \left[\frac{\delta^2}{r_w \rho_e u_e^2}\frac{d(\rho_e u_e^2)}{dx} + \frac{2\delta}{r_w}\frac{d\delta}{dx}\right] - \int_0^{y/\delta} \frac{\rho}{\rho_e}\frac{u}{u_e}\, dy/\delta \left[\frac{u}{u_e}\frac{\delta}{\rho_e u_e}\frac{d(\rho_e u_e)}{dx} + \frac{u}{u_e}\frac{d\delta}{dx} + \frac{u}{u_e}\frac{\delta}{r_w}\frac{dr_w}{dx}\right] + \int_0^{y/\delta} y/\delta \frac{\rho}{\rho_e}\frac{u}{u_e}\, dy/\delta \left[\frac{u}{u_e}\frac{\delta^2}{r_w \rho_e u_e}\frac{d(\rho_e u_e)}{dx} + \frac{u}{u_e}\frac{\delta 2}{r_w}\frac{d\delta}{dx}\right] + \frac{dP_e}{dx}\frac{\delta}{\rho_e u_e^2} y/\delta - \frac{dP_e}{dx}\frac{\delta^2}{r_w}\frac{(y/\delta)^2}{2}\frac{1}{\rho_e u_e^2} \tag{3}$$

Equation (3) allows the determination of $\tau/\rho_e u_e^2$ as a function of y/δ once the various x derivatives and velocity and density profiles are known. Here profiles obtained at station 108 along the wall of the 22-in. Mach 20 helium tunnel are examined (taken from Table 2 of Ref. 5). At this station, small external pressure and wall radius gradients still exist. Input values used in the solution of Eq. (3) include $C_f/2 = 9.75 \times 10^{-5}$, $d\delta/dx = 0.056$, $dr_w/dx = 0.06$, $T_w/T_t = 1.0$ Figure 1 shows results of the calculation. The total shear has been separated into its laminar and turbulent components using the conventional definition of laminar shear. The δ used in the present work is the pitot or density thickness given in Ref. 5. The nominal velocity thickness is much less, as